ACS Photonics

Article

pubs.acs.org/journal/apchd5

Near-Field Thermal Radiation between Metasurfaces

Xianglei Liu and Zhuomin Zhang*

George W. Woodruff School of Mechanical Engineering, Georgia Institute of Technology, Atlanta, Georgia 30332, United States

ABSTRACT: Evanescent waves induced by thermal fluctuations can tunnel through nanoscale gap spacing, leading to super-Planckian thermal radiation. However, investigations of near-field thermal radiation of macroscopic objects have been limited to simple planar or effectively planar geometries until recently. Based on exact formulations including the scattering theory and Green's function method, patterning thin films into 1D and 2D metasurfaces is found to increase the radiative heat flux by more than 1 order of magnitude in a certain range of thicknesses. The underlying mechanism of this counterintuitive phenomenon lies in the excitation of hyperbolic modes supporting high local density of states for broad frequency and *k*-space regimes. The radiative heat flux of a 2D metasurface increases monotonically with the thickness, while the heat flux of a 1D metasurface is not so sensitive to the thickness and is surprisingly higher than that of its 2D counterparts. The stark difference is attributed to the rapid-decay surface modes supported by a 1D metasurface in addition to the slow-decay hyperbolic modes.

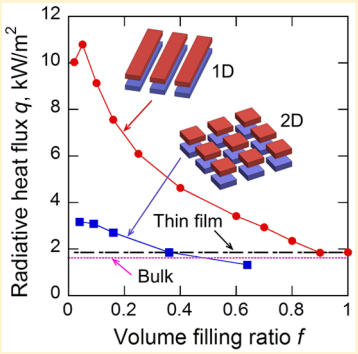

KEYWORDS: *near-field thermal radiation, metasurfaces, hyperbolic modes, nanostructure*

When bringing two or many thermally nonequilibrium objects to the near field, evanescent waves induced by stochastically fluctuating currents will be able to tunnel through the small vacuum gap between them, leading to super-Planckian thermal radiation transfer.[1−9] The experimental confirmation has been made with the gap spacing ranging from tens of nanometers to the submicrometer regime for varying configurations.[10−16] This interesting phenomenon has attracted much attention due to the wide potential applications including but not limited to energy harvesting,[17−20] thermal imaging beyond the diffraction limit,[10,21] and contactless thermal management.[22−28] It is also of great interest for current microelectromechanical systems (MEMS) and nanoelectromechanical systems (NEMS), where nanoscale thermal radiation plays an important role, such as heat dissipation problems in high-power nanoscale electronics. However, theoretical investigations of macroscopic objects have been limited to planar or effectively planar geometries due to the lack of computing techniques[29−34] until recently, when patterned nanostructures are considered based on exact theories.[35−44]

If bulk surface modes such as surface plasmon polaritons (SPPs) and surface phonon polaritons (SPhPs) are excited, the radiative heat flux can be further increased to be orders of magnitude higher than the far-field limit governed by the Stefan−Boltzmann law.[3] However, the frequency band of the resonance-based surface modes is narrow, inhibiting this simple configuration from achieving higher heat flux in certain applications including thermal management, although the efficiency of thermophotovoltaic devices could be better by using narrowband surface modes. One simple method is to employ a thin film, which has been shown to provide a higher near-field heat flux than the bulk counterpart.[14,45−49] The underlying mechanism is attributed to the coupling of surface modes inside the film, which creates additional channels for the photon tunneling. Although the split symmetric and asymmetric coupled modes especially the former can extend to broadband frequencies, the resonance is excited over only a narrow wavevector range.[45,46] Metasurfaces, planar metamaterials with subwavelength thicknesses, have been extensively investigated for far-field manipulation of light propagation, polarization states, and absorption in an unprecedented way[50−54] and have some peculiar advantages over conventional metamaterials, such as less volumetric propagation loss, relative easy fabrication, and compatible integration with other nanodevices. However, their near-field radiative properties have not been investigated. Several groups have calculated near-field radiative heat transfer between structured materials, but rarely considered thin metamaterials. For instance, Guérout et al. theoretically demonstrated enhanced radiative heat transfer of gold nanostructures over bulk gold.[40] Liu et al. proposed to increase near-field radiative heat flux between polar gratings by covering graphene.[38] Chalabi et al. examined the effects of different shapes and the spatially resolved near-field radiative heat flux.[43,44] An open question is whether the radiative heat flux of thin films can be further increased by pattering them into metasurfaces. Based on exact formalisms, the present study theoretically demonstrates that the aforementioned fundamental limitation of being narrow in the *k*-space of surface modes supported by thin films can be overcome to some extent by perforating or patterning them into metasurfaces, so that the radiative heat flux can be further enhanced. In this work, both one-dimensional (1D) and two-dimensional (2D) periodically patterned metasurfaces are considered, and the underlying mechanisms for enhancing near-field radiative transfer are explored.

Received: May 31, 2015
Published: August 17, 2015

DOI: 10.1021/acsphotonics.5b00298
ACS Photonics 2015, 2, 1320−1326

RESULTS AND DISCUSSION

The schematics of near-field thermal radiation for considered 1D and 2D periodic metasurfaces are shown in Figure 1a and b,

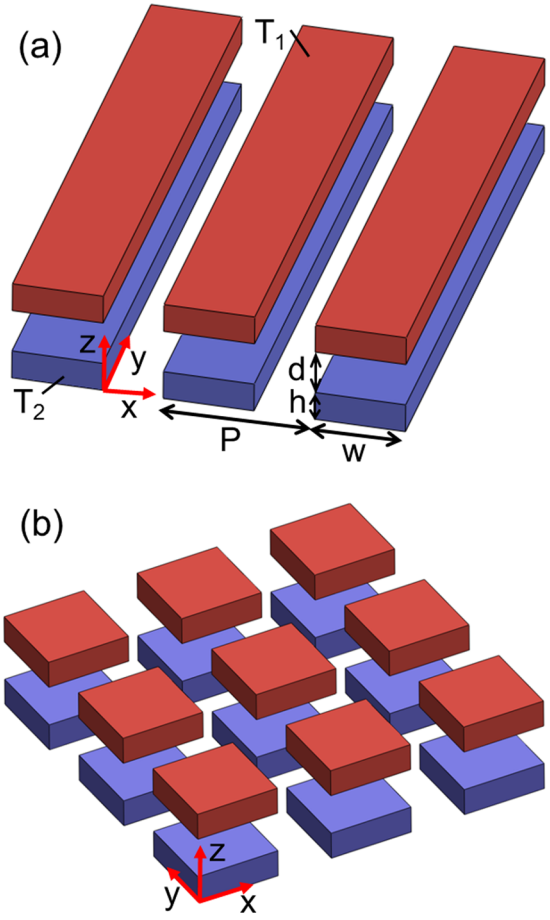

Figure 1. Schematic of near-field radiation between (a) 1D and (b) 2D metasurfaces separated by a vacuum gap of d with temperatures of T_1 and T_2, respectively. Note that h is the thickness, P the period, and W the width of the 1D or 2D patterns.

respectively. The temperatures of the top and bottom metasurfaces, which have identical geometry and are separated by a vacuum gap of d, are T_1 = 310 K and T_2 = 290 K, respectively. The period, width, and thickness of the patterned metasurfaces are denoted by P, W, and h. The unit cell of the 2D metasurface contains a square nanopillar, while that of the 1D metasurface contains a beam extending to infinity in the y direction, i.e., 1D gratings. Doped silicon is used as the base material since SPPs can be thermally excited and the resonance frequency can be tuned by doping.[55] The doping level is set to be 10^{20} cm^{-3}, at which the dielectric function of doped silicon can be described by a Drude model, $\varepsilon(\omega) = \varepsilon_\infty - \omega_p^2/(\omega^2 + i\gamma\omega)$, where ε_∞ is a high-frequency constant of 11.7, ω_p is the plasma frequency of 1.08×10^{15} rad/s, and γ is the scattering rate of 9.34×10^{13} rad/s.[55,56]

Figure 2 gives the radiative heat flux for both configurations with varying volume filling ratios. The volume filling ratio f is defined as W/P and W^2/P^2 for 1D and 2D metasurfaces, respectively. The geometric parameters are taken as P = 100 nm, d = 100 nm, and h = 400 nm. These values are used as a default in this work unless otherwise specified. The radiative heat flux between thin films (f = 1) of the same thickness (h =

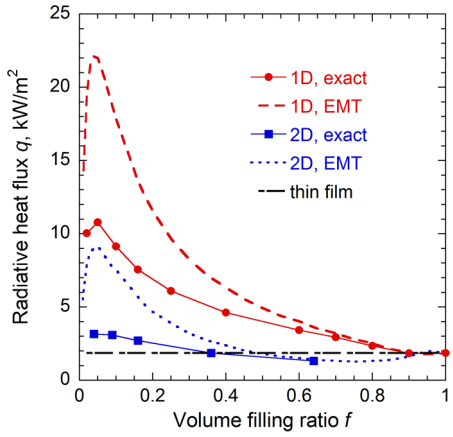

Figure 2. Radiative heat flux as a function of the volume filling ratio at P = 100 nm, d = 100 nm, and h = 400 nm. For all calculations, T_1 = 310 K and T_2 = 290 K.

400 nm) is denoted by the dash-dotted line and is 1860 W/m^2. This value exceeds that between bulk doped silicon of 1629 W/m^2 and is more than 15 times that between blackbodies. The underlying mechanism for the enhancement can be attributed to the coupling of SPPs inside the thin film, as discussed in ref 46, although different materials were used. Patterning the film into a 1D metasurface can enhance thermal radiation for all practical volume filling ratios. Interestingly, while the 2D metasurface yields a radiative heat flux higher than that of thin films at moderate filling ratios, it does not support a heat flux as high as that of the 1D metasurface. Beyond f = 0.36, 2D patterning will deteriorate the radiative transfer as shown in Figure 2. The effective medium theory (EMT) approximation, which is valid only when P is sufficiently small, overpredicts the heat flux for both 1D and 2D configurations. The disagreement between the exact method and EMT is expected to be diminished when reducing the period, as was demonstrated for multilayered metamaterials.[57] The optimal heat flux supported by 1D and 2D metasurfaces reaches 10.79 and 3.17 kW/m^2, respectively. Reducing P is expected to further increase the radiative flux. As indicated by the dashed and dotted curves predicted by EMT, the maximum possible heat flux of 1D and 2D configurations is 22.11 and 9.16 kW/m^2, respectively. These values are about 12 and 5 times as large as that between two films with the same thickness. Therefore, patterned thin metamaterials may increase the heat flux over the counterpart thin films and bulks.

The effects of period are shown in Figure 3 for f = 0.16 with other geometric parameters remaining the same. With decreasing period, the radiative heat flux for both configurations based on exact methods approaches the values predicted by corresponding EMT as expected. As an example, the heat flux of a 2D metasurface at P = 50 nm is 4.26 kW/m^2, which is 25% less than that predicted by EMT. This discrepancy further decreases at small P. At P = 10 nm, the heat flux for 1D metasurface is 13.6 kW/m^2, which is essentially the same as that from EMT. With increasing P, the heat flux decreases and will eventually approach the limit governed by the proximity approximation based on pairwise addition, i.e., the heat flux of thin films multiplied by a factor of f. Metasurfaces support a higher radiative heat flux than thin films unless the period exceeds 900 and 150 nm for 1D and 2D configurations, respectively. Understanding the underlying mechanism of the enhancement enabled by metasurfaces and the reason that a 1D

DOI: 10.1021/acsphotonics.5b00298
ACS Photonics 2015, 2, 1320−1326

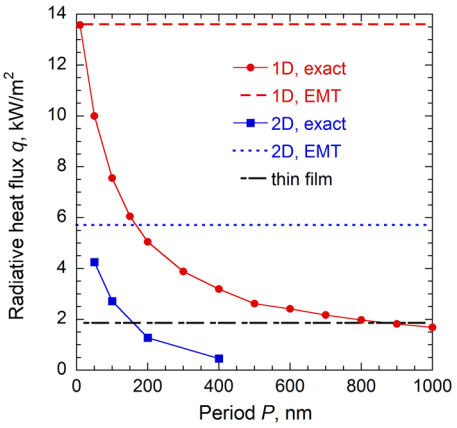

Figure 3. Effects of period on the radiative transfer of metasurfaces for $f = 0.16$, while the other geometric parameters are the same as those for Figure 2.

metasurface has a higher radiative heat flux than the 2D counterpart is necessary before turning this technique into practical applications.

The highest radiative heat flux for metasurfaces occurs when P becomes arbitrarily small when the periodic patterned structures can be homogenized as a thin layer of anisotropic effective medium characterized by EMT. The effective medium corresponding to both 1D and 2D metasurfaces is uniaxial with one distinction that the optical axis of the homogenized 1D effective medium lies horizontally (the y direction) while that for the 2D effective medium lies vertically (the z direction). The effective dielectric functions for ordinary ε_O (electric field is perpendicular to the optical axis) and extraordinary waves (electric field is parallel to the optical axis) ε_E can be calculated using expressions given in ref 57. Then, the dielectric tensor of 1D and 2D effective media is diag(ε_E^{1D},ε_O^{1D},ε_O^{1D}) and diag(ε_O^{2D},ε_O^{2D},ε_E^{2D}), respectively. Since $\varepsilon_E^{1D} = \varepsilon_O^{2D}$ and vice versa for the same filling ratio, in the following, only ε_O and ε_E will be used that are based on 2D metasurfaces. The calculated values for the real parts of ε_O and ε_E as functions of the angular frequency are plotted in Figure 4a for $f = 0.16$ and at a temperature of 300 K. It is assumed that the slight perturbation of temperature for the two metamaterials does not affect their dielectric functions. At frequencies below 2.46×10^{14} rad/s, the dielectric functions of orthogonal directions have opposite signs, implying that a hyperbolic dispersion is supported.[55] Therefore, both 1D and 2D metasurfaces are hyperbolic metamaterials (HMMs) with a thickness of h. For p-polarized electromagnetic waves with high-k, evanescent waves in conventional elliptic materials become propagating. The evanescent waves in the vacuum are coupled with the propagating high-k modes inside the HMM, leading to broadband high local density of states (LDOS).[58] This is the basic mechanism for the efficient radiative transfer supported by 1D and 2D metasurfaces.

To further confirm this scenario, the photon tunneling probability (defined in the Methods section) for a homogenized effective medium of 1D and 2D metasurfaces is shown in Figure 4b and c, respectively. Only p-polarization is considered since waves of s-polarization support neither surface nor hyperbolic modes and thus have negligible contributions for mesoscopic gap distances. As seen from Figure 4b, large photon tunneling probabilities are supported mainly in the hyperbolic region, which has a major contribution to the radiative heat flux

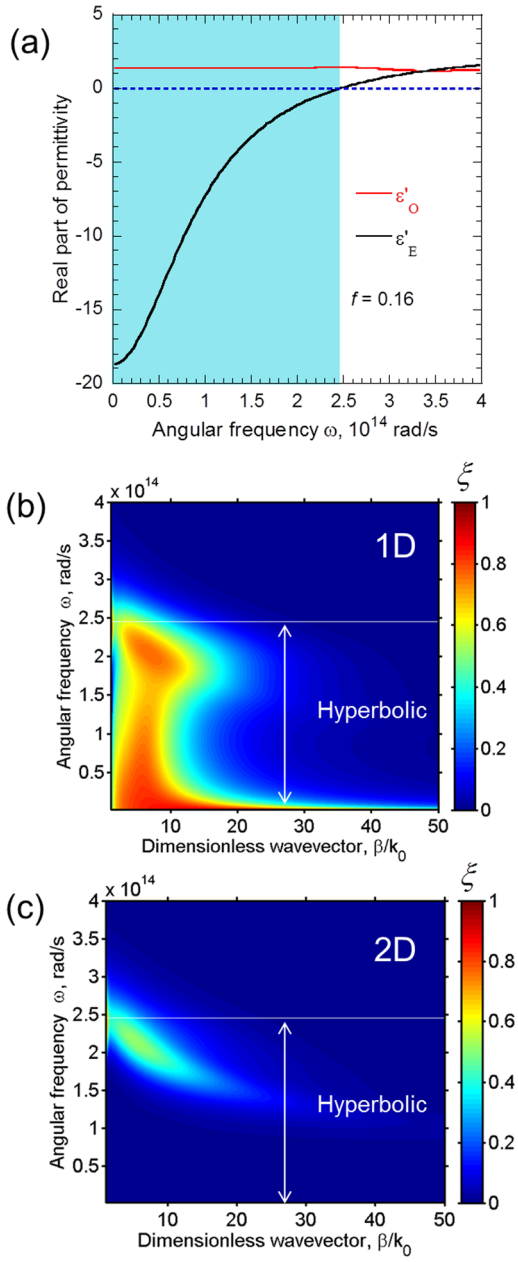

Figure 4. (a) Real part of the effective dielectric function for orthogonal directions for $f = 0.16$. The shaded region supports hyperbolic dispersion. (b) Photon tunneling probability at $d = 100$ nm when the period approaches zero for a 1D thin HMM. (c) 2D thin HMM. The frequency region below the white line is hyperbolic.

between 1D metasurfaces. A similar phenomenon can be found for 2D metasurfaces, as shown in Figure 4c, but the photon tunneling probability at low frequencies is quite small. This is why the 1D metasurface gives rise to a higher heat flux than the 2D counterparts as observed in Figures 2 and 3. At higher frequencies, the imaginary part of $k_{z2D} = (k_0^2\varepsilon_O - \beta^2\varepsilon_O/\varepsilon_E)^{1/2}$ becomes large due to the increase of k_0 and decrease of ε_E; then the field will decay so rapidly that $\exp(2ik_{z2D}h) \to 0$. As a result, a thin 2D HMM behaves as bulk as long as h is not too small.

On the contrary, the photon tunneling probability of 1D thin HMM remains high at low frequencies, as shown in Figure 4b. The longitudinal wavevector inside a 1D HMM is given as[59]

DOI: 10.1021/acsphotonics.5b00298
ACS Photonics 2015, 2, 1320−1326

$$k_{z1D} = \sqrt{\varepsilon_O k_0^2 - \beta^2\left[\cos^2(\varphi) + \frac{\varepsilon_O}{\varepsilon_E}\sin^2(\varphi)\right]} \quad (1)$$

where φ is the angle between the optical axis and the normal of the plane of incidence and should be integrated from 0 to $\pi/2$ to calculate the radiative heat flux.[55] For low frequencies and high-k modes, k_{z1D} becomes $i\beta$ for $\varphi = 0$ and $\beta(\varepsilon_O)^{1/2}/(-\varepsilon_E)^{1/2}$ (the same as k_{z2D}) for $\varphi = \pi/2$. When $\varphi = \pi/2$, k_{z1D} is purely real if losses are not considered, and only purely hyperbolic modes, featured with slow decay, are present. When $\varphi = 0$, k_{z1D} is purely imaginary and, thus, electromagnetic waves are not propagating but evanescent in 1D HMMs, and pure surface modes featuring fast decay are excited due to the negative sign of ε_E. The above two scenarios can be confirmed from the surface resonance dispersion at the interface of a vacuum and the effective anisotropic 1D grating, obtained from the pole of the reflection coefficient as

$$k_{zE}(k_{z0} + k_{zE})(\varepsilon_E k_{z0} k_{z1D} + k_{zE}^2)\sin^2(\varphi) + \varepsilon_E k_0^2(k_{z0} + k_{z1D})(\varepsilon_E k_{z0} + k_{zE})\cos^2(\varphi) = 0 \quad (2)$$

where $k_{zE} = (\varepsilon_E k_0^2 - \beta^2)^{1/2}$ and $k_{z0} = (k_0^2 - \beta^2)^{1/2}$. It can be found that at $\varphi = \pi/2$ eq 2 cannot be satisfied, demonstrating the lack of surface modes. For $\varphi = 0$, eq 2 becomes $k_{z0} + k_{zE}/\varepsilon_E = 0$, which is exactly the same as the dispersion of surface modes at the interface of the vacuum and a homogeneous metallic media characterized by ε_E, and the resonance frequency lies at $\varepsilon_E' = -1$. When φ lies between the two extremes, both hyperbolic and surface modes are supported in 1D HMMs. In general, for any moderate value of φ, the imaginary part of k_{z1D} is larger than that of k_{z2D} due to the small magnitude of $\varepsilon_E^{-1/2}$, resulting in a more rapid decay. Therefore, the penetration depth for 1D thin HMM will be smaller, and a relative insensitivity of the heat flux of 1D thin HMMs to the film thickness compared with 2D thin HMMs is expected.

The thickness effects are shown in Figure 5 for different configurations. The radiative heat flux of 2D thin HMMs increases monotonically with the thickness no matter whether P is equal to 100 nm (exact Green's function method) or approaches zero (EMT limit). As discussed in Figure 4c, the low radiative flux of a 2D thin HMMs at small thicknesses is attributed to the poor photon tunneling at low frequencies. Thin films, on the other hand, tend to have an opposite trend.

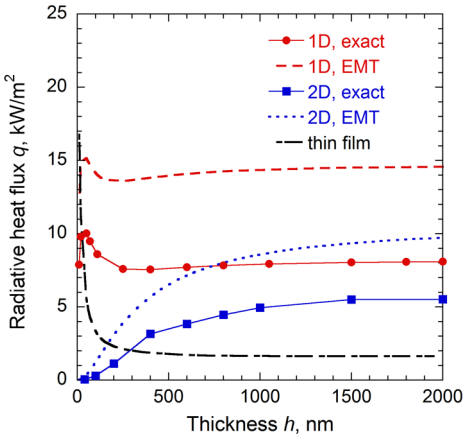

Figure 5. Near-field radiative heat flux as a function of the thickness for different configurations at d = 100 nm.

With decreasing thickness, the radiative heat flux for thin films monotonically increases due to the strengthened coupling of SPPs until the thickness is about 3 nm. For such small thicknesses, patterning thin films into 2D HMMs will not lead to any increase but instead will reduce the heat flux by orders of magnitude compared even with the radiative heat flux of the films multiplied by f, the proximity approximation limit. As confirmed by both exact scattering theory and EMT, the radiative heat flux of 1D thin HMMs has a weak dependence on the thickness due to the small penetration depth. It has a peak at h = 50 nm, which can be attributed to the coupling of surface modes, like thin films. The peak is small since only part of the modes belong to SPPs.

Optimal 1D and 2D HMMs with small periods provide a higher radiative heat flux than thin films when h exceeds 15 and 170 nm, respectively, as indicated by the EMT curves. However, for smaller thicknesses, the radiative heat flux of thin films is the highest. The maximum q at d = 100 nm supported by thin films and 1D HMMs is 24.4 kW/m^2 (h = 3 nm) and 24.0 kW/m^2 (f = 0.04, semi-infinite), respectively. Indeed, the photon tunneling probability approaches the theoretical limit of unity when coupled SPPs are excited though a range over a narrow k-space band.[55] On the other hand, the coupling of high-k waves with the hyperbolic modes is weak although in a broad k-space range. The photon tunneling probability will inevitably exponentially decay with tangential wavevectors since no resonances are excited to offset this decaying trend.[9,47] Nevertheless, this balance is reversed for larger gap spacing. For example, at d = 1000 nm, the maximum q supported by thin films with varying thicknesses is 266 W/m^2, while that for 1D HMM and 2D HMM is 380 and 352 W/m^2, respectively.

CONCLUSION

The near-field radiative heat transfer of 1D and 2D metasurfaces is investigated based on the exact methods and EMT approximation. The photon tunneling probability between thin films is high only when resonances are excited over a narrow k-space regime. Patterning thin films of moderate thicknesses into 1D and 2D metasurfaces can increase the heat flux. The underlying mechanism is due to the excitation of hyperbolic modes featured with high LDOS in a broad frequency and k-space regime. The radiative heat flux for thin 2D HMMs increases monotonically with the thickness, while the heat flux for thin 1D HMMs is not as sensitive to the thickness and is higher than that of 2D HMMs due to the relatively rapid decay of high-k modes supported by surface waves. This work sheds light on the fundamental understanding of thermal radiation between hyperbolic metasurfaces and may pave the way toward applying metasurfaces to achieve effective heat removal from nanodevices, increase the power output of near-field thermophotovoltaic cells, and modulate heat transport contactlessly with a high contrast.

METHODS

The scattering theory and Green's function method are used for 1D and 2D metasurfaces, respectively. In the long-wavelength limit, 1D and 2D metasurfaces can be homogenized as uniaxial materials. Therefore, besides numerical solutions based on the exact formulation, EMT is also employed to show the heat flux in the limit when the period approaches zero.

DOI: 10.1021/acsphotonics.5b00298
ACS Photonics 2015, 2, 1320−1326

A. Scattering Theory Based on Fourier Expansion. The fluctuating electromagnetic field in the vicinity of a hot object including both the propagating and evanescent waves can be given by its scattering properties.[60] Electromagnetic fields in the vacuum gap are determined by multiple scattering of the initially emitted waves. The correlation of fluctuating waves from different objects or different parts of a certain object is diminishing, as essentially indicated by the stochastic electrodynamic theory without considering nonlocal responses.[3,60] Then, the radiative heat flux can be expressed in an elegant way involving only the scattering coefficient of individual objects, which considers both the shape and material dependence.[61] The near-field radiative heat flux between 1D periodic gratings as shown in Figure 1a is given as[60,62]

$$q = \frac{1}{8\pi^3}\int_0^\infty \Theta_{12}(\omega, T_1, T_2)\,\mathrm{d}\omega \int_{-\pi/P}^{\pi/P}\int_{-\infty}^{\infty} \xi(\omega, k_x, k_y) \times \mathrm{d}k_x\,\mathrm{d}k_y \tag{3}$$

where $\Theta_{12}(\omega,T_1,T_2)$ is the difference between the mean energy of Planck oscillators at different temperatures and is given as

$$\Theta_{12}(\omega, T_1, T_2) = \frac{\hbar\omega}{\exp(\hbar\omega/k_B T_1) - 1} - \frac{\hbar\omega}{\exp(\hbar\omega/k_B T_2) - 1} \tag{4}$$

The integration of k_x is exerted over $-\pi/P$ to π/P since all the modes are folded into the first Brillouin zone due to the periodicity in the x direction. The photon tunneling probability or energy transmission coefficient $\xi(\omega,k_x,k_y)$ can be given as[36,40]

$$\xi(\omega, k_x, k_y) = \mathrm{Tr}(\mathbf{D}\mathbf{W}_1\mathbf{D}^\dagger\mathbf{W}_2) \tag{5}$$

$$\mathbf{D} = (\mathbf{I} - \mathbf{S}_1\mathbf{S}_2)^{-1} \tag{6}$$

$$\mathbf{W}_1 = \sum_{-1}^{\mathrm{pw}} -\mathbf{S}_1 \sum_{-1}^{\mathrm{pw}} \mathbf{S}_1^\dagger + \mathbf{S}_1 \sum_{-1}^{\mathrm{ew}} - \sum_{-1}^{\mathrm{ew}} \mathbf{S}_1^\dagger \tag{7}$$

$$\mathbf{W}_2 = \sum_{1}^{\mathrm{pw}} -\mathbf{S}_2^\dagger \sum_{1}^{\mathrm{pw}} \mathbf{S}_2 + \mathbf{S}_2^\dagger \sum_{1}^{\mathrm{ew}} - \sum_{1}^{\mathrm{ew}} \mathbf{S}_2 \tag{8}$$

where $\mathbf{S}_1 = \mathbf{R}_1$, $\mathbf{S}_2 = \mathrm{e}^{ik_{z0}d}\,\mathbf{R}_2\mathrm{e}^{ik_{z0}d}$, † means Hermitian adjoint, and $\mathbf{D}$ is a Fabry–Pérot-type matrix considering multiple scatterings inside the vacuum cavity. Here, $\mathbf{R}_1$ and $\mathbf{R}_2$ are the reflection coefficient matrices of $(4N + 2) \times (4N + 2)$ for the top and bottom grating, respectively, and N is the diffraction order used in the Fourier expansion. Those reflection coefficient matrices consider geometry effects and are obtained based on Fourier space expansion. Operators $\sum_{-1(1)}^{\mathrm{pw(ew)}}$ identifying propagating and evanescent modes have been presented in refs 36, 38, and 40.

B. Green's Function Method. The scattering theory method presented in Section A, mainly used for 1D periodic metamaterials, can be extended to arbitrary 2D periodic metamaterials, but the memory requirement for convergence will increase tremendously. Therefore, for thermal radiation of 2D metasurfaces as shown in Figure 1b, the direct Green's function method is used here. It is well known that the emitted electromagnetic waves are induced by the fluctuating currents, which could be quantized and related to the susceptibility of the system according to the fluctuation–dissipation theory pioneered by Rytov and co-workers.[36] The correlation function of random fluctuating currents in an anisotropic, local, and nonmagnetic medium reads[61]

$$\langle J_i(\mathbf{r}, \omega)\, J_k^*(\mathbf{r}', \omega')\rangle = \frac{4\omega\varepsilon_0\Theta(\omega, T)\,\varepsilon_{ik}''(\mathbf{r}, \omega)}{\pi}\delta(\mathbf{r} - \mathbf{r}')\,\delta(\omega - \omega') \tag{9}$$

where ε_0 is the vacuum permittivity, ε_{ik}'' is the imaginary part of the dielectric tensor component, and the Dirac delta functions indicate spatial and temporal incoherence. The electric and magnetic fields are determined by the corresponding dyadic Green's functions and fluctuating currents as[1,3,61,63]

$$E(\mathbf{r}, \omega) = j\omega\mu_0 \int_{V'} \overline{\overline{G}}^E(\mathbf{r}, \mathbf{r}', \omega)\, J(\mathbf{r}', \omega)\,\mathrm{d}V' \tag{10}$$

$$H(\mathbf{r}, \omega) = \int_{V'} \overline{\overline{G}}^H(\mathbf{r}, \mathbf{r}', \omega)\, J(\mathbf{r}', \omega)\,\mathrm{d}V' \tag{11}$$

After some lengthy derivations based on eqs 9–11, the near-field radiative heat flux between the two metamaterials can be expressed as

$$q = \frac{2k_0^2}{\pi}\int_0^\infty \Theta_{12}(\omega, T_1, T_2)\,\mathrm{d}\omega \times \int_{V'} \mathrm{Re}\Big[j\sum_{i=x,y,z}\varepsilon_{ii}''(\omega)(G_{xi}^E G_{yi}^{H*} - G_{yi}^E G_{xi}^{H*})\Big]\,\mathrm{d}V' \tag{12}$$

where k_0 is the wavevector in the vacuum and V' is the source region (emitter). Equation 12 can be generally applied to arbitrary nanostructures with known tensors of permittivity once the dyadic Green's functions are obtained. One way to calculate Green's functions is using the finite-difference time-domain (FDTD) method (e.g., Lumerical Solutions, Inc.) based on a brute-force approach. Pulsed sources are placed in an ergodic method, and then the corresponding dyadic Green's functions are determined by dividing the Fourier transform of the induced time-dependent electric and magnetic fields by the transform of the current sources.[64,65] The Ricker wavelet, the second derivative of the Gaussian pulse, is used as the source, as recommended by Didari and Mengüç.[64] The reason is that it does not have any direct current component, which usually causes nonphysical artifacts and thus leads to computational errors.

C. Local Effective Medium Theory. When the gap distance is much larger than the period, local EMT based on homogenizing metamaterials as an anisotropic effective medium becomes fairly accurate.[64] Equation 3 can be used for predicting the radiative heat flux for arbitrary anisotropic materials with a modification that the integral range of k_x becomes unlimited just like k_y. Since only the specular scattering needs to be considered, the photon tunneling probability can be expressed in a simpler way as[57]

$$\xi(\omega, k_x, k_y) = \begin{cases} \mathrm{Tr}[(\mathbf{I} - \mathbf{R}_2^*\mathbf{R}_2)\mathbf{D}(\mathbf{I} - \mathbf{R}_1\mathbf{R}_1^*)\mathbf{D}^*], \beta < k_0 \\ \mathrm{Tr}[(\mathbf{R}_2^* - \mathbf{R}_2)\mathbf{D}(\mathbf{R}_1 - \mathbf{R}_1^*)\mathbf{D}^*]\mathrm{e}^{-2|k_{z0}|d}, \beta > k_0 \end{cases} \tag{13}$$

where $\beta = (k_x^2 + k_y^2)^{1/2}$ is the magnitude of the tangential wavevector. The 2×2 Fresnel reflection coefficient matrix for

DOI: 10.1021/acsphotonics.5b00298
ACS Photonics 2015, 2, 1320–1326

incidence from the vacuum to the medium i = 1 or 2 is expressed as

$$\mathbf{R}_i = \begin{bmatrix} r_{ss}^i & r_{sp}^i \\ r_{ps}^i & r_{pp}^i \end{bmatrix} \quad (14)$$

The element r_{sp}^i represents the case of cross-polarization when an incident wave with s-polarization becomes p-polarized after being reflected by medium i, and this rule applies to the other three terms. These reflection coefficients can be obtained by applying boundary conditions that tangential electric and magnetic fields are continuous across each interface. For uniaxial media with the optical axis lying vertically (2D metasurfaces) or horizontally (1D metasurfaces), explicit expressions of reflection coefficients can be found in refs 2 and 66. When the optical axis lies vertically, nondiagonal terms representing the polarization coupling effects are diminishing.

AUTHOR INFORMATION

Corresponding Author

*E-mail: zhuomin.zhang@me.gatech.edu.

Notes

The authors declare no competing financial interest.

ACKNOWLEDGMENTS

The research is mainly supported by the U.S. Department of Energy, Office of Science, Basic Energy Sciences (DE-FG02-06ER46343). Z.M.Z. would also like to thank the support of the National Science Foundation (CBET-1235975).

REFERENCES

(1) Joulain, K.; Mulet, J. P.; Marquier, F.; Carminati, R.; Greffet, J. J. Surface electromagnetic waves thermally excited: Radiative heat transfer, coherence properties and Casimir forces revisited in the near field. *Surf. Sci. Rep.* **2005**, *57*, 59−112.

(2) Biehs, S.-A.; Ben-Abdallah, P.; Rosa, F. S. Nanoscale radiative heat transfer and its applications. *Infrared Radiation*; Morozhenko, V., Eds.; InTech: Rijeka, Croatia, 2012; Chapter 1.

(3) Zhang, Z. M. *Nano/Microscale Heat Transfer*; McGraw-Hill: New York, 2007.

(4) Liu, X. L.; Wang, L. P.; Zhang, Z. M. Near-Field Thermal Radiation: Recent Progress and Outlook. *Nanoscale Microscale Thermophys. Eng.* **2015**, *19*, 98−126.

(5) Shen, S. Experimental studies of radiative heat transfer between bodies at small separations. *Annu. Rev. Heat Transfer* **2013**, *16*, 327−343.

(6) Jones, A. C.; O'Callahan, B. T.; Yang, H. U.; Raschke, M. B. The thermal near-field: Coherence, spectroscopy, heat transfer, and optical forces. *Prog. Surf. Sci.* **2013**, *88*, 349−392.

(7) Xuan, Y. An overview of micro/nanoscaled thermal radiation and its applications. *Photon. Nanostr. Fundam. Appl.* **2014**, *12*, 93−113.

(8) Cahill, D. G.; Braun, P. V.; Chen, G.; Clarke, D. R.; Fan, S.; Goodson, K. E.; Keblinski, P.; King, W. P.; Mahan, G. D.; Majumdar, A.; Maris, H. J.; Phillpot, S. R.; Pop, E.; Shi, L. Nanoscale thermal transport. II. 2003−2012. *Appl. Phys. Rev.* **2014**, *1*, 011305.

(9) Liu, X. L.; Zhang, R. Z.; Zhang, Z. M. Near-perfect photon tunneling by hybridizing graphene plasmons and hyperbolic modes. *ACS Photonics* **2014**, *1*, 785−789.

(10) Kittel, A.; Muller-Hirsch, W.; Parisi, J.; Biehs, S. A.; Reddig, D.; Holthaus, M. Near-field heat transfer in a scanning thermal microscope. *Phys. Rev. Lett.* **2005**, *95*, 224301.

(11) Shen, S.; Narayanaswamy, A.; Chen, G. Surface Phonon Polaritons Mediated Energy Transfer between Nanoscale Gaps. *Nano Lett.* **2009**, *9*, 2909−2913.

(12) Ottens, R. S.; Quetschke, V.; Wise, S.; Alemi, A. A.; Lundock, R.; Mueller, G.; Reitze, D. H.; Tanner, D. B.; Whiting, B. F. Near-Field Radiative Heat Transfer between Macroscopic Planar Surfaces. *Phys. Rev. Lett.* **2011**, *107*, 014301.

(13) Kralik, T.; Hanzelka, P.; Zobac, M.; Musilova, V.; Fort, T.; Horak, M. Strong Near-Field Enhancement of Radiative Heat Transfer between Metallic Surfaces. *Phys. Rev. Lett.* **2012**, *109*, 224302.

(14) Song, B.; Ganjeh, Y.; Sadat, S.; Thompson, D.; Fiorino, A.; Fernández-Hurtado, V.; Feist, J.; Garcia-Vidal, F. J.; Cuevas, J. C.; Reddy, P.; Meyhofer, E. Enhancement of near-field radiative heat transfer using polar dielectric thin films. *Nat. Nanotechnol.* **2015**, *10*, 253−258.

(15) St-Gelais, R.; Guha, B.; Zhu, L.; Fan, S.; Lipson, M. Demonstration of Strong Near-Field Radiative Heat Transfer between Integrated Nanostructures. *Nano Lett.* **2014**, *14*, 6971−6975.

(16) Babuty, A.; Joulain, K.; Chapuis, P.-O.; Greffet, J.-J.; De Wilde, Y. Blackbody Spectrum Revisited in the Near Field. *Phys. Rev. Lett.* **2013**, *110*, 146103.

(17) DiMatteo, R. S.; Greiff, P.; Finberg, S. L.; Young-Waithe, K. A.; Choy, H. K. H.; Masaki, M. M.; Fonstad, C. G. Enhanced photogeneration of carriers in a semiconductor via coupling across a nonisothermal nanoscale vacuum gap. *Appl. Phys. Lett.* **2001**, *79*, 1894−1896.

(18) Park, K.; Basu, S.; King, W. P.; Zhang, Z. M. Performance analysis of near-field thermophotovoltaic devices considering absorption distribution. *J. Quant. Spectrosc. Radiat. Transfer* **2008**, *109*, 305−316.

(19) Francoeur, M.; Vaillon, R.; Mengüç, M. P. Thermal Impacts on the Performance of Nanoscale-Gap Thermophotovoltaic Power Generators. *IEEE Trans. Energy Convers.* **2011**, *26*, 686−698.

(20) Narayanaswamy, A.; Chen, G. Surface modes for near field thermophotovoltaics. *Appl. Phys. Lett.* **2003**, *82*, 3544−3546.

(21) Jones, A. C.; Raschke, M. B. Thermal infrared near-field spectroscopy. *Nano Lett.* **2012**, *12*, 1475−1481.

(22) Otey, C. R.; Lau, W. T.; Fan, S. Thermal rectification through vacuum. *Phys. Rev. Lett.* **2010**, *104*, 154301.

(23) Yang, Y.; Basu, S.; Wang, L. Radiation-based near-field thermal rectification with phase transition materials. *Appl. Phys. Lett.* **2013**, *103*, 163101.

(24) Ben-Abdallah, P.; Biehs, S.-A. Near-field thermal transistor. *Phys. Rev. Lett.* **2014**, *112*, 044301.

(25) Zhu, L.; Otey, C. R.; Fan, S. Ultrahigh-contrast and large-bandwidth thermal rectification in near-field electromagnetic thermal transfer between nanoparticles. *Phys. Rev. B: Condens. Matter Mater. Phys.* **2013**, *88*, 184301.

(26) Wang, L. P.; Zhang, Z. M. Thermal rectification enabled by near-field radiative heat transfer between intrinsic silicon and a dissimilar material. *Nanoscale Microscale Thermophys. Eng.* **2013**, *17*, 337−348.

(27) Gu, W.; Tang, G.-H.; Tao, W.-Q. Thermal switch and thermal rectification enabled by near-field radiative heat transfer between three slabs. *Int. J. Heat Mass Transfer* **2015**, *82*, 429−434.

(28) Huang, J. G.; Li, Q.; Zheng, Z. H.; Xuan, Y. M. Thermal rectification based on thermochromic materials. *Int. J. Heat Mass Transfer* **2013**, *67*, 575−580.

(29) Biehs, S. A.; Tschikin, M.; Ben-Abdallah, P. Hyperbolic metamaterials as an analog of a blackbody in the near field. *Phys. Rev. Lett.* **2012**, *109*, 104301.

(30) Liu, X. L.; Zhang, R. Z.; Zhang, Z. M. Near-field thermal radiation between hyperbolic metamaterials: Graphite and carbon nanotubes. *Appl. Phys. Lett.* **2013**, *103*, 213102.

(31) Drosdoff, D.; Phan, A. D.; Woods, L. M. Transverse electric mode for near-field radiative heat transfer in graphene−metamaterial systems. *Adv. Opt. Mater.* **2014**, *2*, 1038−1042.

(32) Bai, Y.; Jiang, Y.; Liu, L. Role of surface plasmon polaritons on the enhancement of the near-field thermal radiation from fishnet metamaterial. *J. Phys. D: Appl. Phys.* **2014**, *47*, 445304.

DOI: 10.1021/acsphotonics.5b00298
ACS Photonics 2015, 2, 1320−1326

(33) Guo, Y.; Cortes, C. L.; Molesky, S.; Jacob, Z. Broadband super-Planckian thermal emission from hyperbolic metamaterials. *Appl. Phys. Lett.* **2012**, *101*, 131106.
(34) Chang, J.-Y.; Basu, S.; Wang, L. Indium tin oxide nanowires as hyperbolic metamaterials for near-field radiative heat transfer. *J. Appl. Phys.* **2015**, *117*, 054309.
(35) Rodriguez, A. W.; Ilic, O.; Bermel, P.; Celanovic, I.; Joannopoulos, J. D.; Soljačić, M.; Johnson, S. G. Frequency-selective near-field radiative heat transfer between photonic crystal slabs: a computational approach for arbitrary geometries and materials. *Phys. Rev. Lett.* **2011**, *107*, 114302.
(36) Lussange, J.; Guérout, R.; Rosa, F. S. S.; Greffet, J. J.; Lambrecht, A.; Reynaud, S. Radiative heat transfer between two dielectric nanogratings in the scattering approach. *Phys. Rev. B: Condens. Matter Mater. Phys.* **2012**, *86*, 085432.
(37) Otey, C. R.; Zhu, L.; Sandhu, S.; Fan, S. Fluctuational electrodynamics calculations of near-field heat transfer in non-planar geometries: A brief overview. *J. Quant. Spectrosc. Radiat. Transfer* **2014**, *132*, 3−11.
(38) Liu, X. L.; Zhang, Z. M. Graphene-assisted near-field radiative heat transfer between corrugated polar materials. *Appl. Phys. Lett.* **2014**, *104*, 251911.
(39) Liu, X. L.; Zhao, B.; Zhang, Z. M. Enhanced near-field thermal radiation and reduced Casimir stiction between doped-Si gratings. *Phys. Rev. A: At., Mol., Opt. Phys.* **2015**, *91*, 062510.
(40) Guérout, R.; Lussange, J.; Rosa, F. S. S.; Hugonin, J. P.; Dalvit, D. A. R.; Greffet, J. J.; Lambrecht, A.; Reynaud, S. Enhanced radiative heat transfer between nanostructured gold plates. *Phys. Rev. B: Condens. Matter Mater. Phys.* **2012**, *85*, 180301.
(41) Liu, B.; Shen, S. Broadband near-field radiative thermal emitter/absorber based on hyperbolic metamaterials: Direct numerical simulation by the Wiener chaos expansion method. *Phys. Rev. B: Condens. Matter Mater. Phys.* **2013**, *87*, 115403.
(42) Liu, B.; Liu, Y.; Shen, S. Thermal plasmonic interconnects in graphene. *Phys. Rev. B: Condens. Matter Mater. Phys.* **2014**, *90*, 195411.
(43) Chalabi, H.; Hasman, E.; Brongersma, M. L. Near-field radiative thermal transfer between a nanostructured periodic material and a planar substrate. *Phys. Rev. B: Condens. Matter Mater. Phys.* **2015**, *91*, 014302.
(44) Chalabi, H.; Hasman, E.; Brongersma, M. L. Effect of shape in near-field thermal transfer for periodic structures. *Phys. Rev. B: Condens. Matter Mater. Phys.* **2015**, *91*, 174304.
(45) Biehs, S. A. Thermal heat radiation, near-field energy density and near-field radiative heat transfer of coated materials. *Eur. Phys. J. B* **2007**, *58*, 423−431.
(46) Francoeur, M.; Mengüç, M. P.; Vaillon, R. Near-field radiative heat transfer enhancement via surface phonon polaritons coupling in thin films. *Appl. Phys. Lett.* **2008**, *93*, 043109.
(47) Miller, O. D.; Johnson, S. G.; Rodriguez, A. W. Effectiveness of thin films in lieu of hyperbolic metamaterials in the near field. *Phys. Rev. Lett.* **2014**, *112*, 157402.
(48) Fu, C. J.; Tan, W. C. Near-field radiative heat transfer between two plane surfaces with one having a dielectric coating. *J. Quant. Spectrosc. Radiat. Transfer* **2009**, *110*, 1027−1036.
(49) Francoeur, M.; Mengüç, M. P.; Vaillon, R. Coexistence of multiple regimes for near-field thermal radiation between two layers supporting surface phonon polaritons in the infrared. *Phys. Rev. B: Condens. Matter Mater. Phys.* **2011**, *84*, 075436.
(50) Kildishev, A. V.; Boltasseva, A.; Shalaev, V. M. Planar photonics with metasurfaces. *Science* **2013**, *339*, 1232009.
(51) Dabidian, N.; Kholmanov, I.; Khanikaev, A. B.; Tatar, K.; Trendafilov, S.; Mousavi, S. H.; Magnuson, C.; Ruoff, R. S.; Shvets, G. Electrical switching of infrared light using graphene integration with plasmonic fano resonant metasurfaces. *ACS Photonics* **2015**, *2*, 216−227.
(52) Aydin, K.; Ferry, V. E.; Briggs, R. M.; Atwater, H. A. Broadband polarization-independent resonant light absorption using ultrathin plasmonic super absorbers. *Nat. Commun.* **2011**, *2*, 517.
(53) Alali, F.; Kim, Y. H.; Baev, A.; Furlani, E. P. Plasmon-enhanced metasurfaces for controlling optical polarization. *ACS Photonics* **2014**, *1*, 507−515.
(54) Campione, S.; Guclu, C.; Ragan, R.; Capolino, F. Enhanced magnetic and electric fields via fano resonances in metasurfaces of circular clusters of plasmonic nanoparticles. *ACS Photonics* **2014**, *1*, 254−260.
(55) Liu, X. L.; Zhang, R. Z.; Zhang, Z. M. Near-field radiative heat transfer with doped-silicon nanostructured metamaterials. *Int. J. Heat Mass Transfer* **2014**, *73*, 389−398.
(56) Shi, J.; Li, P.; Liu, B.; Shen, S. Tuning near field radiation by doped silicon. *Appl. Phys. Lett.* **2013**, *102*, 183114.
(57) Liu, X. L.; Bright, T. J.; Zhang, Z. M. Application conditions of effective medium theory in near-field radiative heat transfer between multilayered metamaterials. *J. Heat Transfer* **2014**, *136*, 092703.
(58) Cortes, C. L.; Newman, W.; Molesky, S.; Jacob, Z. Quantum nanophotonics using hyperbolic metamaterials. *J. Opt.* **2012**, *14*, 063001.
(59) Liu, X. L.; Wang, L. P.; Zhang, Z. M. Wideband tunable omnidirectional infrared absorbers based on doped-silicon nanowire arrays. *J. Heat Transfer* **2013**, *135*, 061602.
(60) Bimonte, G.; Santamato, E. General theory of electromagnetic fluctuations near a homogeneous surface in terms of its reflection amplitudes. *Phys. Rev. A: At., Mol., Opt. Phys.* **2007**, *76*, 013810.
(61) Rytov, S. M.; Kravtsov, Y. A.; Tatarskii, V. I. *Principles of Statistical Radiophysics*; Springer: New York, 1989.
(62) Krüger, M.; Bimonte, G.; Emig, T.; Kardar, M. Trace formulas for nonequilibrium Casimir interactions, heat radiation, and heat transfer for arbitrary objects. *Phys. Rev. B: Condens. Matter Mater. Phys.* **2012**, *86*, 115423.
(63) Narayanaswamy, A.; Zheng, Y. A Green's function formalism of energy and momentum transfer in fluctuational electrodynamics. *J. Quant. Spectrosc. Radiat. Transfer* **2014**, *132*, 12−21.
(64) Didari, A.; Mengüç, M. P. Analysis of near-field radiation transfer within nano-gaps using FDTD method. *J. Quant. Spectrosc. Radiat. Transfer* **2014**, *146*, 214−226.
(65) Datas, A.; Hirashima, D.; Hanamura, K. FDTD simulation of near-field radiative heat transfer between thin films supporting surface phonon polaritons: lessons learned. *J. Therm. Sci. Technol.* **2013**, *8*, 91−105.
(66) Biehs, S.-A.; Rosa, F. S. S.; Ben-Abdallah, P. Modulation of near-field heat transfer between two gratings. *Appl. Phys. Lett.* **2011**, *98*, 243102.

DOI: 10.1021/acsphotonics.5b00298
ACS Photonics 2015, 2, 1320−1326